# A Wideband Beamforming Antenna Array for 802.11ac and 4.9 GHz in Modern Transportation Market

Moh Chuan Tan, Minghui Li, *Member, IEEE*, Qammer H. Abbasi, *Senior Member, IEEE*, and Muhammad Ali Imran, *Senior Member, IEEE*

***Abstract*—In this work, a novel antenna structure has been proposed, which consists of multiple sub-array features i.e., a field selectable beam (90°, 180°, 270°, and 360°) and the choice of gain (11.16, 14.59 and 17.25 dBi) that can be easily adapted to cater for the dynamic scenarios in the transportation environment. The sub-arrays were designed using the microstrip patch antenna (MPA) concept with capacitive feed and dual substrate stacked up configuration for superior operating bandwidth covering the entire 802.11ac (5.17 to 5.85 GHz Industrial Scientific and Medical (ISM) band), in addition to the extended coverage for 4.92 to 4.98 GHz licensed band with narrow azimuth beamwidth of 24°. The sub-array was designed, simulated and experimentally evaluated and the beamforming results revealed that the antenna structure can be integrated with beamforming concepts to provide an enhanced wireless link between the ground base station and the mobile terminals that allows beam steering to focus on the targeted direction and null the interference directions with small beam width. It is expected that the proposed configurable gain/beam beamforming antenna array will further reduce the deployment cost and enhance the anti-interference performance by two-fold, and shall bring the user experience in the transportation market to the next level.**

***Index Terms*—Smart antenna, wideband antenna, beamforming, broadband communication.**

## I. Introduction

THE advancement of broadband wireless technologies such as Long Term Evolution (LTE), 5G, and 802.11ac, Multiple Input Multiple Output (MIMO) technologies has improved the lifestyle of the users with broadband-enabled devices such as the smartphone, personal digital assistant (PDA), etc. Applications such as direct video streaming on the move and transmission of high throughput data between mobile terminals and the base station become possible. This has drawn tremendous interest in the industrial sector in order to provide efficient and reliable wireless infrastructure to cater for the increase in the market demand as well as to catch up with the higher expectation in user experience perspective.

Transportation market is one area that benefits mostly from the advanced wireless technology. We can imagine how good the experience is, if the mobile users can enjoy the seamless data streaming connectivity while transporting from point A to point B using various modes of transports such as a car, bus, train, ship etc. Increases in the wireless infrastructure have led to serious airspace congestion, especially in the license-free spectrum such as 2.4 GHz and 5 GHz Industrial Scientific and Medical (ISM) and 4.9 GHz licensed band. It's essential to have a smart infrastructure that can adapt itself to the highly congested environment. The configurable antenna structure with smart antenna concepts comes in as a right candidate aimed to harmonize the congested wireless environment. The antenna structure that can be preconfigured to different gain and coverage sectors comes with beamforming capability that steers the beam towards the targeted client and nulls to the interference. Adaptive beamforming can be implemented and further enhanced by iterating the beamformer weights on-the-fly, whose phase and amplitude can be altered in real time according to the environment.

In this work, the focused application area is on the wireless link between cars and the road-side base stations and between trains to the trackside base stations with fixed access points serving multiple mobile clients in the unlicensed 802.11ac and licensed 4.9 GHz band. In the mobile environment, the antenna beam for the mobile terminals and base stations are not always fixed. In the traditional access point deployment [1], both the access point and the mobile client are equipped with the omni-directional antenna to provide a total of 360° coverage. The potential challenges with the traditional deployment are, i) more access points are needed due to the small cell radius, ii) mutual interference between adjacent cells, iii) high deployment cost to lay cables, poles, power, etc. and iv) high maintenance cost due to more equipment. The proposed antenna structure along with the smart antenna technique is set to overcome those challenges.

In the volatile transportation environment, different application scenarios may require different physical coverage beam and communication range as illustrated in Fig. 1, for example, an access point installed at the track-side of a single track may

Manuscript received May 22, 2019; revised September 2, 2019, November 4, 2019, and December 18, 2019; accepted December 22, 2019. Date of publication December 31, 2019; date of current version March 12, 2020. This work was supported in part by the EPSRC Global Challenges Research Fund, DARE Project EP/P028764/1. The review of this article was coordinated by Dr. Yue Gao. *(Corresponding author: Moh Chuan Tan; Minghui Li.)*

M. C. Tan is with the RFNet Technologies Pte. Ltd., Singapore 319319, and also with the University of Glasgow, Glasgow, G12 8QQ Scotland, United Kingdom (e-mail: tmohchuan@rfnetech.com).

M. Li, Q. H. Abbasi, and M. A. Imran are with the James Watt School of Engineering, University of Glasgow, G12 8QQ Glasgow, United Kingdom (e-mail: david.li@glasgow.ac.uk; qammer.abbasi@glasgow.ac.uk; muhammad.imran@glasgow.ac.uk).

Digital Object Identifier 10.1109/TVT.2019.2963111

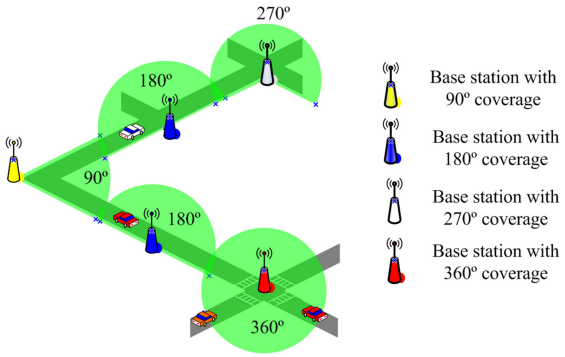


Fig. 1. Zone coverage for various application scenarios in vehicular environment.

require 180° coverage instead of 360°, a right-angle road turn may require just 90° beam coverage. In addition, the antenna gain of choice can be chosen from the low/mid/high gain arrays to match the application needs. Furthermore, each array in the proposed antenna structure was designed with beamforming capability for integration with beamforming front-end. This method allows optimum interference performance and lowest deployment and maintenance cost to suit the volatile transportation environment. The proposed antenna structure with beamforming capability can perform as good as the conventional smart antenna and reconfigurable antenna with added following benefits, i) lower cost and no waste materials (only desired arrays are installed), ii) good field maintainability with fewer components, iii) faster processing time, thus lesser processing power (only need to focus on the dedicated sectors) and iv) further interference reduction (only radiate and scan on the array installed).

The literature review has been carried out in the following 3 areas, smart beamforming antenna, phase array that formed the smart antenna structure and individual antenna elements that reside in the phase array. Many works had been carried out in the smart antenna arena and mostly centered around the beamforming and reconfigurable structure, therefore, we proposed a practical approach to integrate the wideband antenna arrays into the antenna system that is suitable for deployment in the various vehicular application scenarios. A reconfigurable beam and polarization antenna was proposed in [2] operating in 5 beams within 0° to 360° and 3 polarizations (orthogonal or diagonal linear polarizations) operating in 2.4 GHz, the reconfigurable mechanism was achieved by switching the bias voltage over the PIN diodes on the polarization reconfigurable square patch and the parasitic elements. Similarly, in [3], a reconfigurable dual polarized beam switching antenna was proposed using radial waveguides excited by central probes and feeding multiple radiating elements, 36 PIN diodes were loaded to reconfigure the polarization and the radiating beam in the wireless local area network (WLAN) 5 GHz band (5.18–5.825 GHz). Another reconfigurable beam in the elevation plane [4] was reported using the slotted array and driven by the PIN diode for LTE femtocells, the achieved down-tilt angles were 13° and 32°, respectively with approximately 3 dB beamwidth. In [5], the reconfiguration beam switching smart antenna was proposed using the radiating patch with six parasitic elements switches by PIN diodes, azimuth beamwidth of 42° and reconfigurable to six directions over 360° were achieved. The reconfigurable techniques [2]–[5] are among the popular techniques, where the beam switching was commonly driven by PIN diodes, however, such technique has its disadvantages to migrate into digital beamforming systems, where the high precision steering angle and interference nulling are required. In this work, we are aiming for a wideband antenna structure that can be preconfigured to different gain and coverage beam, which is highly demanded in the dynamic transportation environment.

The phase array is one of the important components in our proposed configurable structure, however the beam steering antenna array proposed in literature seems to be centered around the application fields such as 5G [6]. [12]–[16], X-band [17], LTE [19], 2.4 GHz ISM band using Butler matrix technique [20], and 2.35 GHz to 2.8 GHz/5 GHz to 5.5 GHz $1 \times 4$ beam steerable antenna array [21]. In the 802.11ac area, there were many good pieces of literature works in the past which mainly focused on enhancing the antenna array structure but still lagging of ability to cover the entire wide operating band from 4.9 to 5.9 GHz. For example, a dual polarization $2 \times 4$ antenna structure [22] has been proposed with 12 dBi peak gain and the operating band from 5150 to 5850 MHz, and in [23], a 5 GHz band patch antenna is loaded with the Complementary Split Ring Resonators (CSRR) for miniaturization, lower gain of $-0.16$ dBi and limited 80 MHz operating bandwidth (BW). Similarly, in [24], the 8 elements MIMO antenna with 6.5 dBi gain serving narrow frequency bandwidth from 4.985 to 5.15 GHz has been proposed. Furthermore, in [25], an antenna array with 3 monopole patches, inverted L and inverted Z with slightly wider bandwidth covering 5 to 6 GHz with a gain from 2 to 3.7 dBi is proposed. In this work, we will introduce the wideband and high-gain phase arrays that operate from 4.9–5.9 GHz band for usage in the proposed antenna structure.

The characteristics of the antenna array are highly depending on the type of antenna element used. The Microstrip Patch Antenna (MPA) [7] is a very common antenna element used in mobile and automotive devices due to its low cost, flexible structure, and simplicity in design and manufacture. The conventional MPA usually comes with a lower gain and a narrow operating bandwidth ratio. Many works have been carried out to overcome the gain and operation bandwidth limitation of the conventional MPA. A wideband multilayer patch antenna [8] was proposed, and the structure was able to achieve 14% bandwidth ratio, however, this may not be suitable for large array integration in term of manufacturability due to the nature of the stacked capacitive coupling through air structure. Techniques such as Electromagnetic BandGap (EBG) [9] and Defective Ground Structure (DGS) [11] have successfully improved the bandwidth ratio to 18.68% and 63.65%, however, the size was the disadvantage. An open slot was introduced on the radiating patch [10] to enhance the bandwidth ratio to 22% but with a lower gain of around 3.25 dBi. In [18], an ultra-wideband dual substrate MPA with a small capacitive feed was proposed with close to 50% BW ratio and more than 7 dBi gain, the

TABLE I
GLOSSARY OF NOTATIONS

| | |
|---|---|
| $W$ | Width of the patch |
| $L$ | Length of the patch |
| $\Delta L$ | Extended length of the patch |
| $f_r$ | Center frequency |
| $\mu_o$ | Magnetic permeability of free space |
| $\varepsilon_o$ | Electric permeability of free space |
| $\varepsilon_r$ | Dielectric constant of the substrate |
| $c$ | Speed of light |
| $\varepsilon_{reff}$ | Effective dielectric constant |
| $t$ | Length of the capacitive feed |
| $s$ | Width of the capacitive feed |
| $d$ | Distance of capacitive feed to patch |
| $g$ | Thickness of the airgap |

capacitive coupling was realized by the spacing between the feeding patch and the radiating patch on the same PCB layer that increases the manufacturability of the antenna, this can be a potential candidate for further optimization and integration into a beamforming array.

In this work, we propose a novel antenna structure and the method to develop a flexible and practical beamforming antenna system that can provide the following features, which were not presented before in literature to the best knowledge of the authors:

a) Wide frequency range covering the entire 802.11ac range 5.17 to 5.85 GHz (ISM band) and 4.92 to 4.98 GHz (License Band) that was realized by MPA on the dual layers of thick substrate consisting of air and the F4BTM-2 material.
b) Choice of gain 11.16, 14.59 and 17.25 dBi can be chosen from the prefabricated $1 \times 4$, $2 \times 4$ and $4 \times 4$ arrays.
c) Selectable sector, which can be configured to support 90°/180°/270°/360° coverage with up to 4 units of the array with 90° sector coverage each.
d) Beam steering capability with 24° beamwidth.

The paper is organized as follows. Section II presents the design approach for the antenna structure, a single element MPA is designed and then the multiple elements are integrated into the antenna array. Section III presents the simulation and experimental results for the proposed MPA element and the antenna arrays, and then the performance parameters are verified with the design specifications. Section IV demonstrates the beamforming performance of the antenna array, and the key performances are summarized and compared with the relevant state-of-the-art antennas. Section V concludes the paper. Table I lists the main notations used in this paper.

## II. ANTENNA ARRAY DESIGN

The antenna array design process is presented as follows. In Section II-A, the antenna element was simulated and fabricated, the wide bandwidth and high gain were achieved by the dual substrate and capacitive feeding structure. In Section II-B, the elements were integrated into an antenna array that was designed with optimum element separation. The antenna feeding network

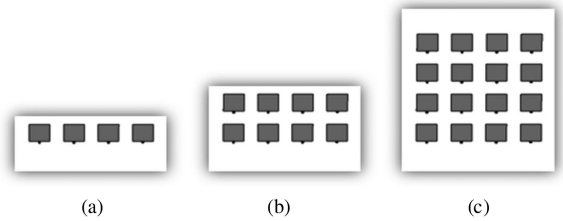


Fig. 2. Antenna array with different gain. (a) Low gain. (b) Medium gain. (c) High gain.

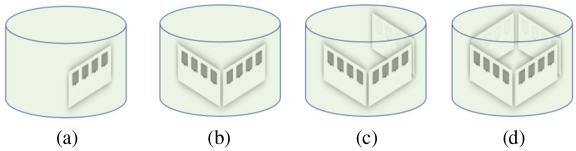


Fig. 3. Antenna array with different beam. (a) 90° beam. (b) 180° beam. (c) 270° beam. (d) 360° beam.

was designed to properly match the antenna elements to the feeding ports in Section III-C.

The proposed variable gain and radiating beam wideband antenna array was established based on the following specifications, a wide operating frequency range covering the entire 4.9 to 5.9 GHz with less than 10 dB return loss, a selectable gain (low, medium and high), and the 90° beam steering capability per each array.

The antenna array consists of multiple MPA elements designed with high gain and wide operating bandwidth which are achieved by deploying the capacitive feed MPA on the dual substrate structure. The proposed arrays can be easily configured for different gain and beam coverage angle to achieve the best configuration needed for the volatile transportation environment where different application scenarios may require different physical coverage beam and communication range.

Firstly, the wideband high-gain antenna element was designed, and then the antenna array was formed by following the 2 simple configuration steps. The first step is shown in Fig. 2 allowing the modular antenna elements and the feed network to be constructed to form a sub-array with a different gain that supports 90° beam steering. And the second step is shown in Fig. 3 allowing the simple integration of multiple sub-modules to form the beam coverage of 90°, 180°, 270°, and 360°; similarly, the middle-gain and high-gain antenna array can be configured in the same way using the respective sub-array.

### *A. Antenna Array Element Design and Optimization*

The proposed antenna arrays consist of multiple elements arranged in a horizontal and vertical manner. The dual substrate capacitive coupling feed method [18] was adopted in this design due to its wideband, high gain and manufacture-friendly characteristics. The radiator is represented by the larger patch and the energy is fed using a small capacitive patch via capacitive coupling. The capacitive feed method can reduce the mismatch between the radiating patch and the co-axial feed, and the dual

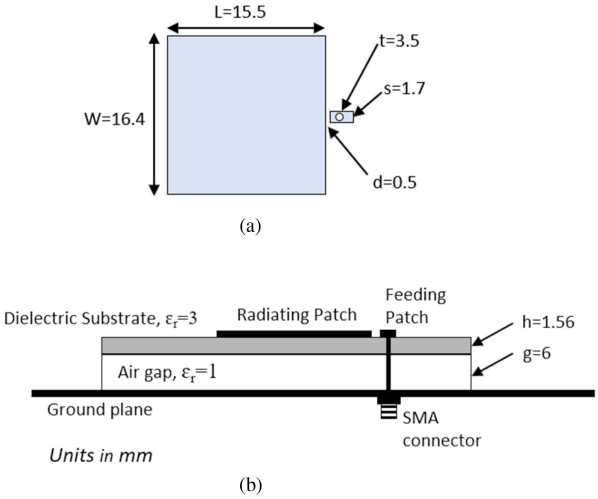


Fig. 4. Capacitive feed dual-substrate MPA. (a) Top view. (b) Cross-sectional view.

dielectric substrate layers will enhance the gain and BW of the MPA. The antenna is designed to resonate at 5.5 GHz on a substrate F4BTM-2 with relative permittivity, $\varepsilon_{\mathrm{r}} = 3$, and the dimension of the patch $L$ and $W$ were calculated using [7],

$$W = \frac{1}{2f_r\sqrt{\mu_o\varepsilon_o}}\sqrt{\frac{2}{\varepsilon_r+1}} = \frac{c}{2f_r}\sqrt{\frac{2}{\varepsilon_r+1}} \tag{1}$$

where $W$ is the width of the patch, $f_r$ is the center frequency, $\mu_o$ and $\varepsilon_o$ are referring to the magnetic and electric permeability of free space, $\varepsilon_r$ is the dielectric constant of the substrate and $c$ is the speed of light.

$$L = \frac{c}{2f_r\sqrt{\varepsilon_{reff}}} - 2\Delta L \tag{2}$$

where $L$ is the length of the patch, $\varepsilon_{reff}$ is the effective dielectric constant and $\Delta L$ is the extended length of the patch that can be calculated using equations (3) and (4).

$$\varepsilon_{reff} = \frac{\varepsilon_r+1}{2} + \frac{\varepsilon_r-1}{2}\left[1+12\frac{h}{W}\right]^{-\frac{1}{2}} \tag{3}$$

where $h$ is the height of the substrate.

$$\Delta L = 0.412h\frac{(\varepsilon_{reff}+0.3)\left(\frac{W}{h}+0.264\right)}{(\varepsilon_{reff}-0.258)\left(\frac{W}{h}+0.8\right)} \tag{4}$$

The capacitive feed length ($t$), width ($s$), distance to patch ($d$), and the space of airgap ($g$) can be optimized to achieve the optimum frequency bandwidth. In this work, the design of [18] was optimized for wider operating bandwidth to cover the entire 4.9–5.9 GHz frequency range with less than 10 dB returned loss, and higher gain between 7.42 and 8.69 dBi; as a result, about 15% improvement in both bandwidth and gain were achieved through parameter optimization against the simulated results from the original design parameter in [18].

Fig. 4 shows the geometrical model with the optimized parameters for the capacitive feed MPA. The antenna parameters were optimized and simulated using the Computer Simulation Technology (CST) Studio Suite (Darmstadt, Germany) [29]. The simulation results are presented in Section III.

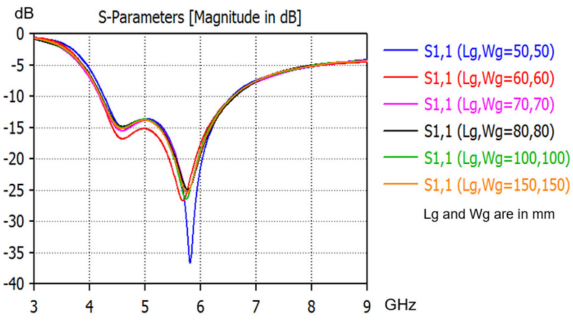


Fig. 5. Effect of different size of the ground plane.

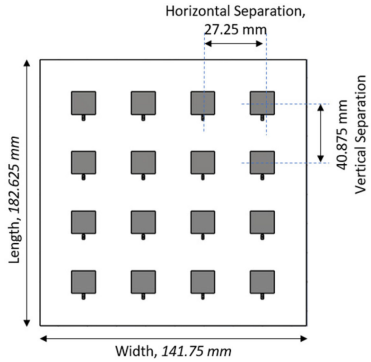


Fig. 6. Illustration of the array in "Far Field" simulation.

Given the fact that the ground plane will be increased when the antenna element is integrated into a bigger array, the return loss performance was evaluated with respect to the different size of the ground plane, and the results are presented in Fig. 5 where Lg and Wg represent the length and width of the ground plane. The results show that the increase in the size of the ground plane does not impact the performance, thus the proposed element is suitable to be integrated into a large antenna array.

### B. Beamforming Antenna Array Design and Optimization

Antenna arrays are very versatile and are used to synthesize a required pattern that cannot be achieved with a single element [26] where the element spacing need to be properly optimized for optimum performance in gain, side lobe, and beamwidth. Prior to the integration of the single element into the array, the array performance was evaluated using CST simulations [29] as shown in Fig. 6. The gain, side lobe and beamwidth performance of the proposed $4 \times 4$ antenna array with respect to the element separation are presented in Fig. 7 and Fig. 8.

The gain and beamwidth performances are plotted in Fig. 7. It was observed that the antenna array's gain increases when the element separation increases, the maximum gain of 21 dBi was observed at the element spacing of 46.025 mm which is slightly less than $1\lambda$ (wavelength). On the other hand, the beamwidth decreases exponentially when the element spacing increases, for example, at 20 mm element separation, the beamwidth decreases by 30% for every 10 mm increases in the element separation,

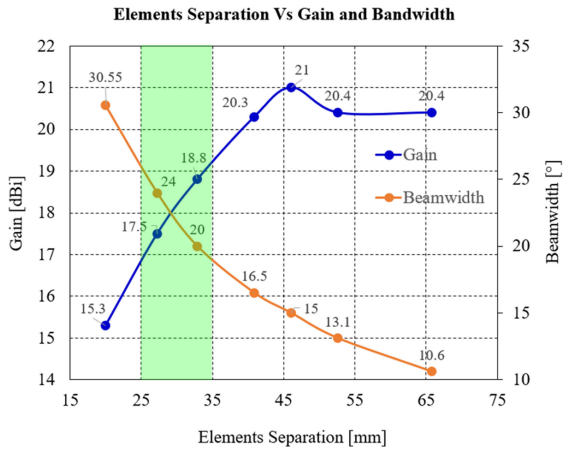


Fig. 7. Gain and beamwidth performance with respect to element separation.

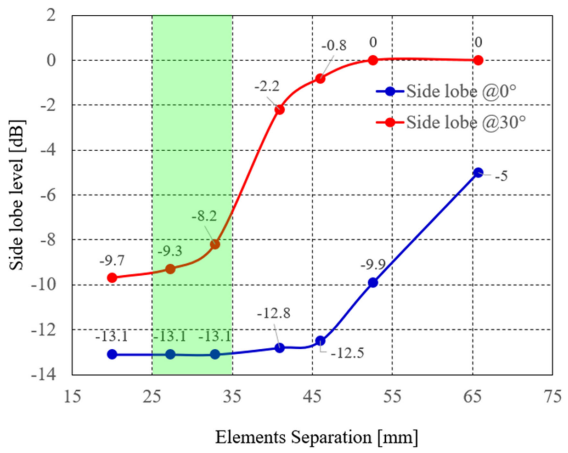


Fig. 8. Maximum sidelobe level at 0° and 30° beam angle with respect to element separation.

22% at 30 mm element separation, 18% at 40 mm element separation and so on.

Fig. 8 demonstrates the sidelobe performance at 0° and 30° beam direction with respect to the element spacing. 30° is used as an example when the beam is steered, and other angles are expected to subject to similar effects. It was observed that at 0° beam, the maximum achievable side lobe is −13.1 dB, the side lobe increases for wider element separations and when the beam steered. When the element separation was increased further to 1λ spacing, the grating lobe appeared, two end-fire maxima were created. From this result, we conclude that the horizontal element separation should keep below 35 mm in order to maintain a reasonable sidelobe level.

From the results, it can be seen that there is a trade-off between the gain, sidelobe, and beamwidth, and the shaded green zone in Fig. 7 and Fig. 8 is the possible element separation to be considered. In our application that focuses on horizontal beam steering, the traditional 27.25 mm (½λ) horizontal element separation was chosen for the good side lobe and gain performance, and 40.875 mm (¾λ) vertical separation was chosen for the optimum gain and beamwidth, in addition, wider vertical separation will reduce

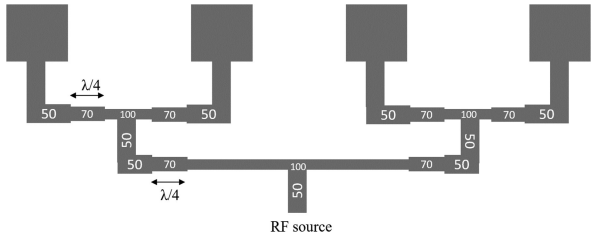


Fig. 9. Corporate feed design.

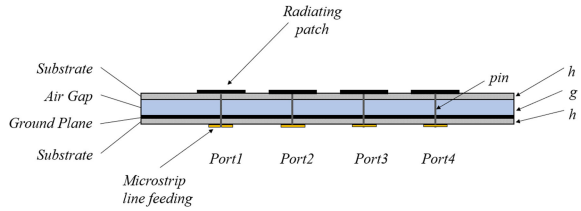


Fig. 10. Construction of the n × 4 antenna array with the microstrip feed.

the mutual coupling between the antenna elements. The simulated performance is summarized as follows, gain = 17.5 dBi, beamwidth = 24°, sidelobe @ 0° beam = −13.1 dB and sidelobe @ 30° beam = −9.3 dB. The design is also applicable to other applications that do not require antenna beam steering such as the point to point antenna, where the antenna separation of 45 mm can be chosen for high gain (21 dBi), small beamwidth (15°) and reasonable side lobe (−12.5 dB).

### *C. Design of the Feeding Network for the Beamforming Antenna Array*

Once the antenna element spacing is defined, the next step is to design the antenna microstrip feeding network to combine all vertical elements into a single feed vertical array. 4 of these vertical arrays will then be arranged horizontally to form a $n \times 4$ beamforming array. The antenna element can be fed by a single line (series feed) or multiple lines (corporate feed) [26]. The series feed is simple, but it's limited to the array with fixed beams, furthermore, any changes in one of the elements or the feed line will affect the performance of others such as mutual coupling and internal reflections. On the contrary, the corporate feed is flexible and ideal for beam scanning phase arrays. In this work, we will focus on corporate feed. The *n* numbers of vertical elements are combined via microstrip feed at the bottom layer using a ¼λ impedance transform to create a single feed vertical array. The geometry of the 1 × 4 vertical array realized by the corporate feed with a quarter wavelength impedance transform method is shown in Fig. 9.

The proposed antenna array is constructed from the dual substrate stacked up as illustrated in Part A. The feeding network is introduced at the opposite side of the ground plane using the substrate F4BTM-2 with $\varepsilon_r = 3$ and thickness = *h*, and the mutual element coupling can be eliminated by separating the radiating element and the feeding network with a ground plane. The cross-sectional view of the proposed $n \times 4$ antenna array construction is shown in Fig. 10.

The design parameters are tabulated in Table II Three types of antenna arrays were created, i.e., 1 × 4 (4 elements), 2 × 4

TABLE II
DESIGN PARAMETERS FOR THE 4 × 4 ANTENNA ARRAY

| Parameter | Description | Value |
|---|---|---|
| *h* | The thickness of the substrate | 1.56 mm |
| *g* | The thickness of the air-substrate | 6 mm |
| *y* | Horizontal separation of the antenna element | 27.25 mm |
| *x* | Vertical separation of the antenna element | 40.875 mm |
| *Lant* | Length of the 1 × 4 antenna array<br>Length of the 2 × 4 antenna array<br>Length of the 4 × 4 antenna array | 60 mm<br>100.875 mm<br>182.625 mm |
| *Want* | Width of the antenna array | 141.75 mm |
| $\varepsilon_r$ | Relative permittivity of the substrate material | 3 |

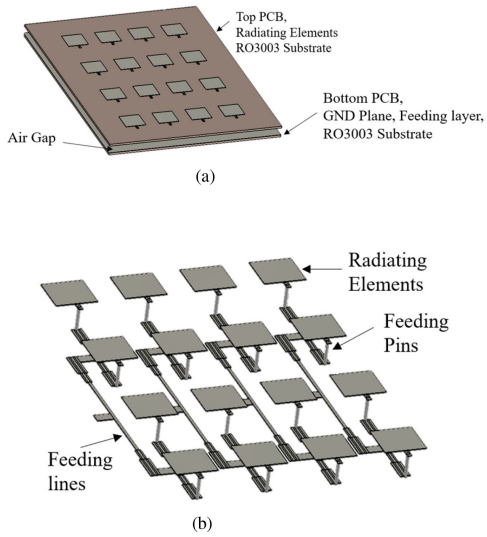


Fig. 11. Antenna PCB stack up and exploded view. (a) Stack up view of the 4 × 4 array. (b) Exploded view of the 4 × 4 array.

(8 elements) and 4 × 4 (16 elements). The horizontal separation between the elements is 27.25 mm, and the vertical separation is 40.875 mm. All the 3 types of antenna arrays have the same width of 141.75 mm and different length, i.e., 60 mm for the 1 × 4 array, 100.875 mm for the 2 × 4 array and 182.625 mm for the 4 × 4 array. The antenna arrays were then simulated using the CST simulation tool, and the simulation results are presented in the next section.

## III. ANTENNA ARRAY PERFORMANCE VALIDATION

The antennas are fabricated using the commercial PCB fabrication technique, and the raw PCBs are assembled according to the stack up sequences shown in Fig. 11 to form the antenna array. The conducted and radiated performances of the single element and the antenna array are measured and reported in this section.

### A. Antenna Fabrication

The proposed antenna arrays are fabricated and experimentally evaluated. The antenna arrays consist of 2 pieces of PCB, the top side PCB contains the radiating elements etched over the F4BTM-2 substrate. The second PCB contains the feeding

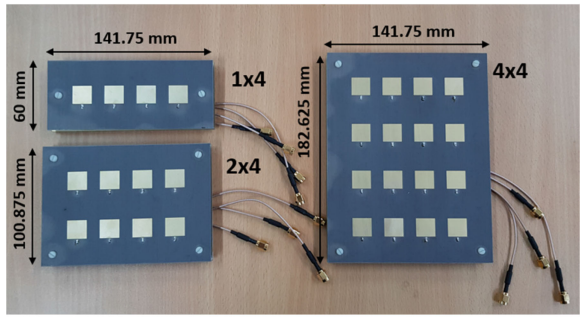


Fig. 12. Top view of the fabricated antenna arrays.

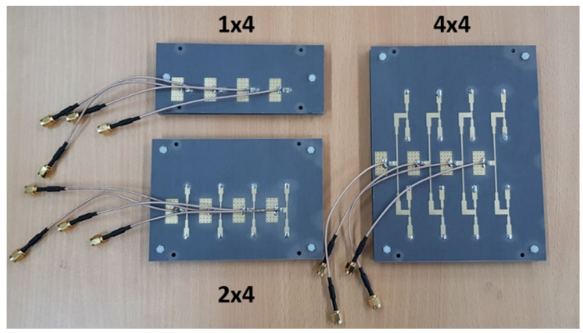


Fig. 13. Bottom view of the fabricated antenna arrays.

network etched over the F4BTM-2 substrate with the opposite side as a solid ground plane. Fig. 11 shows the overview of the PCB stack up and the exploded view of the antenna construction. Both PCBs can be assembled by stacking up using the rigid feeding pins and the additional nylon screw can be installed to strengthen the structure.

For cost reasons, the lower cost substrate material F4BTM-2 from Taizhou Wangling (Jiangsu, China) was chosen, where 60% cost saving was expected compared to the well-known RO3003 material [7], [14] and [18] from Roger (Arizona, United States) with similar electrical specifications. The fabricated PCB is assembled with the shield of the coaxial cable soldered to the ground plate and the signal pin soldered to the antenna feed point as shown in Fig. 13, the coaxial cable is terminated with the SMA connectors to facilitate the experimental measurement. as shown in Fig. 12 (the top view of the assembled antenna arrays) and Fig. 13 (the bottom view of the assembled antenna array).

### B. Measurement Results

The returned loss of the antenna arrays was evaluated for the individual port. The measurements were done using the vector network analyzer (VNA) VNA0406 e-SB from MegiQ (Eindhoven, Netherlands). The measured results are presented in Fig. 14 where (a) is for the 1 × 4 array, (b) for the 2 × 4 array and (c) for the 4 × 4 array. All the antennas were measured with the returned loss of less than 10 dB for the frequency band from 4.9 to 5.9 GHz. There was a noticeable shift in the 1st resonance frequency at around 4.5 GHz, which may be due to the manufacturing tolerance of the PCB stack up and the SMA connectors. However, the measured returned loss was able to achieve the returned loss of less than 10 dB across the

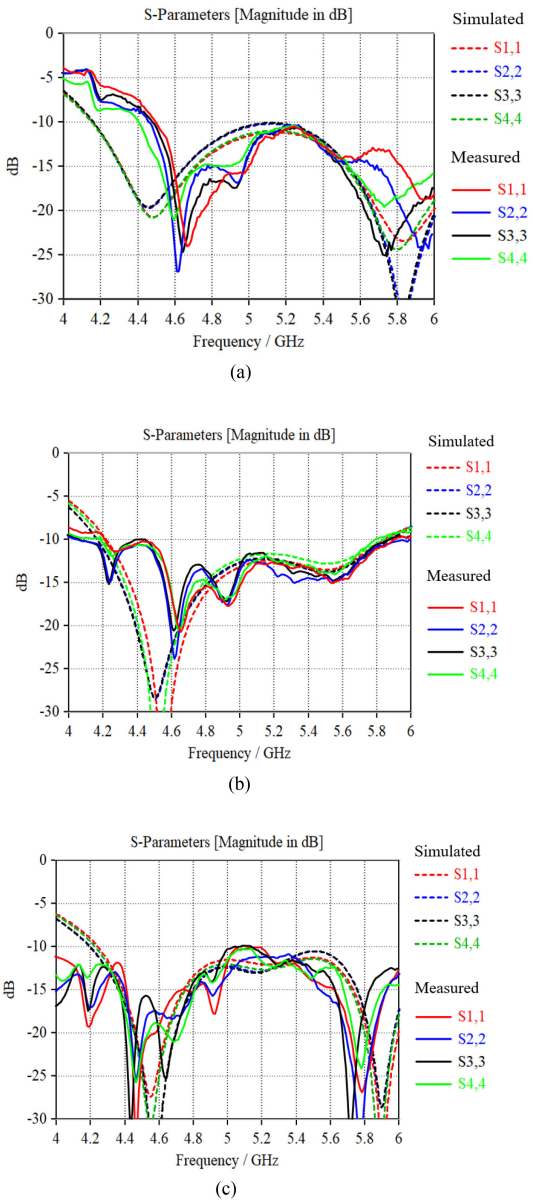


Fig. 14. Returned loss measurement results. (a) Returned loss of the 1 × 4 array. (b) Returned loss of the 2 × 4 array. (c) Returned loss of the 4 × 4 array.

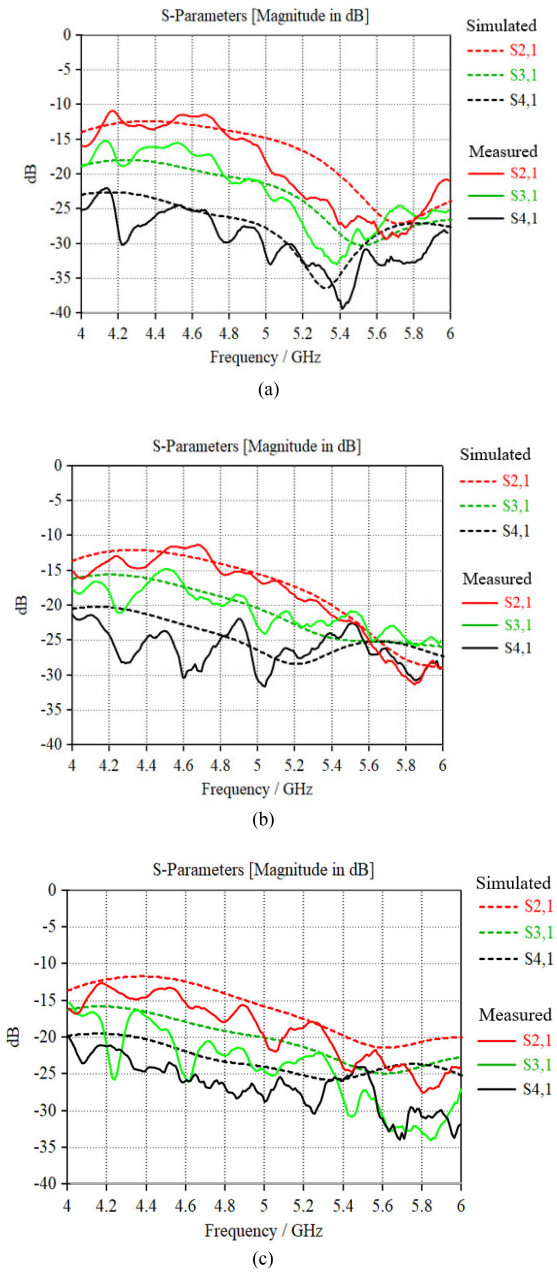


Fig. 15. Measured and simulated inter-port isolation. (a) Inter-port isolation of the 1 × 4 array. (b) Inter-port isolation of the 2 × 4 array. (c) Inter-port isolation of the 4 × 4 array.

whole desired operating frequency range from 4.9 to 5.9 GHz, which fulfilled the minimum returned loss requirement set in our antenna design.

The inter-port isolation was measured and compared with the simulated results. Due to the symmetricity, only the isolation between port 1 and the rest of the ports is shown, the isolation for other ports is similar to the curves in Fig. 15. Moderate agreement was observed between the simulations and measured results, this was mainly due to the manufacturing and stack up tolerance of the antenna PCB. However, the fair isolation performance was obtained in our array design, the inter-port isolation of minimum 15 dB between 4.9 and 5.4 GHz and more than 20 dB between 5.4 and 5.9 GHz is achieved which is a reasonable value to eliminate the crosstalk between the antenna elements.

### C. Radiated Measurement Results

The realized gain of the antenna arrays can be measured using the measurement topology presented in Fig. 16(a) In this section, the antenna array was experimentally evaluated at its nominal 0° beam. A power splitter is used to split the Radio Frequency (RF) source generated from the signal source into 4 antenna ports with the equal phase to excite the RF beam in the direction of 0° towards the radiating plane.

*1) Antenna Radiated Measurement Topology:* The antenna radiated performance was measured by adopting the free space technique presented in [27] and the Free Space Loss (FSL) as described in [28]. Thus, using the Friis equation for free space,

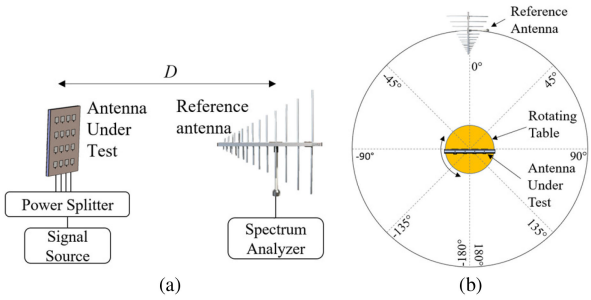


Fig. 16. Antenna measurement setup and orientation. (a) Measurement setup. (b) Antenna orientation.

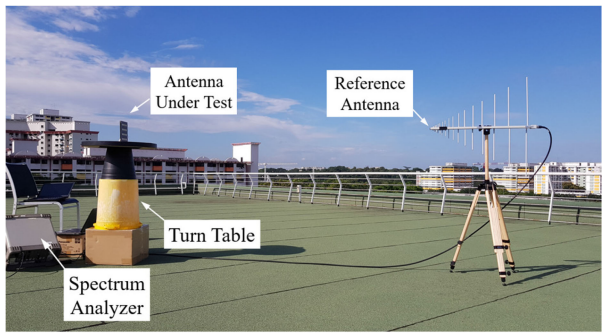


Fig. 17. Actual antenna measurement setup.

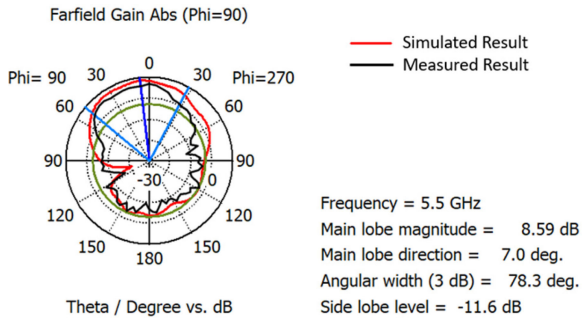


Fig. 18. The measurement results of the radiation pattern of the single element antenna.

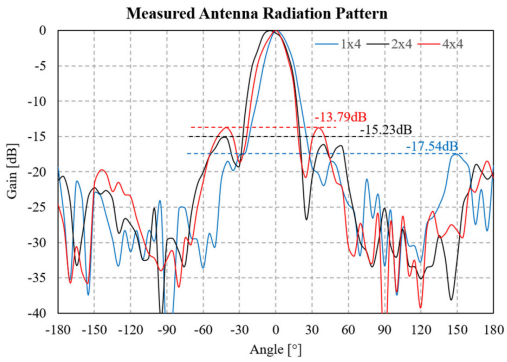


Fig. 19. The measurement results of the radiation patterns of the antenna arrays.

the received antenna gain can be derived as follows:

$$G_r + G_t = 20 \log \left( \frac{4\pi f D}{c} \right) + P_r - P_t + \alpha \qquad (5)$$

where $G_r$ and $G_t$ are the realized gain in (dB) of the receiver (reference antenna) and transmitter antenna (antenna under test), $f$ is the frequency of interest, $D$ is the distance between the transmitter and the receiver and $c$ is the speed of light ($3 \times 10^8$ m/s), $P_r$ is the received power in (dBm), $P_t$ is the transmitted power in (dBm), and $\alpha$ is the attenuation factor due to the cable or connector loss.

A log periodic reference antenna part number: LP-04, manufactured by Narda (Milano, Italy) with the gain provided by the manufacturer being 6 dBi at 5.5 GHz is used to measure the radiated power from the antenna under test, and the source signal was generated by an in-house IEEE802.11an wireless module that was pre-calibrated to provide 23 dBm RF power output at the frequencies of interest. The spectrum analyzer E4407B from Agilent (Santa Clara, United States) was used to measure the power received at the receiver antenna. In our measurement, we set $D = 3$ meters, the FSL was calculated to 56.79 dB, the attenuation factor $\alpha$ was pre-measured using a golden antenna set, and was pre-calculated and offset into the subsequent measurement.

The geometry of the antenna under test is shown in Fig. 16(b) The reference antenna is fixed at one direction, and the antenna under test is placed vertically with reference to the horizontal plane, and the measurement of the 360° radiation pattern can be obtained by constantly rotating the antenna under test by 5° step over 360° in the horizontal plane. The RF strength received by the spectrum analyzer is recorded and further computed using equation (5) to obtain the realized gain and the radiation pattern of the antenna under test. To minimize the measurement errors due to the indoor reflection, the open site at the building top was selected as our measurement site. Refer to Fig. 17, the photo captured at the actual measurement site.

*2) Radiation Results for Single Element Antenna:* The far field radiation pattern of the single element antenna is presented in Fig. 18, the measured radiating beamwidth is around 80°, which agrees well with the simulation results. The realized gain for 4.9/5.5/5.9 GHz is 7.3/6.87/5.5 dBi respectively compared to the simulated gain of 7.42/8.59/8.69 dBi, where a noticeable lower gain was observed at the higher frequency, which was probably due to the frequency response of the SMA connectors and cable.

*3) Radiation Results for Antenna Arrays:* The measured results of the radiation patterns for the $1 \times 4$, $2 \times 4$ and $4 \times 4$ antenna arrays at 5.5 GHz and 0° beam are shown in Fig. 19, and the antenna parameters including the realized gain, sidelobe level, and 3 dB beamwidth are captured and tabulated in Table III where the results are compared with the simulated results.

As shown in Table III and Fig. 19, the measured antenna gains are 11.16 dBi for the $1 \times 4$ array, 14.59 dBi for $2 \times 4$ array and 17.25 dBi for $4 \times 4$ array, which agreed well with the simulated results with some minor delta that is probably due to the environmental factors, connector tolerance as well as the manufacturing tolerance of the PCB patch antennas. Further gain measurements are done at other frequencies from 4.9 to 5.9 GHz

TABLE III
ANTENNA ARRAY MEASURED RESULT VS SIMULATED RESULT

| | | | 1 × 4 | 2 × 4 | 4 × 4 |
|---|---|---|---|---|---|
| Antenna Gain | dBi | Simulated | 13.53 | 15.4 | 17.8 |
| | | Measured | 11.16 | 14.59 | 17.25 |
| Sidelobe Level | dB | Simulated | - 12.9 | - 13.8 | - 13.6 |
| | | Measured | - 17.54 | - 15.23 | - 13.79 |
| 3dB Beamwidth | ° | Simulated | 24.4° | 24.3° | 24.5° |
| | | Measured | 20° | 24° | 20° |

with the gain measured 11.16 to 12.27 dBi for the 1 × 4 array, 13.97 to 15.74 dBi for 2 × 4 array and 17.25 to 18.12 dBi for 4 × 4 array, where the arrays demonstrate a less than 2 dB gain delta across the operating frequencies. Moderate agreement was observed when compared with the simulation result of 12.90 to 14.10 dBi for 1 × 4 array, 15.00 to 15.70 dBi for 2 × 4 array and 17.40 to 18.40 for 4 × 4 array. The measured results also revealed that the sidelobe level of the antenna is better than the simulated results, for example, the 1 × 4 array sidelobe was measured −17.54 dB compared to the simulated result of −12.9 dB. This is potentially due to the manufacturing tolerance of the PCB patch antenna that caused lower antenna gain compared to the simulation results, thus lowering the sidelobe level. The measurement results of the 3 dB beamwidth of less than 24° was also agreed well with the simulated result. When comparing the 2 × 4 array with the state-of-the-art 1 × 8 array of the same number of elements [16], the proposed array structure exhibits a higher gain of 13.97 to 15.74 dBi at 0° beam compared with ∼ 6.9 dBi in [16] and both arrays have a low sidelobe level of < −10 dB, thus, the proposed array structure with 1 × 4, 2 × 4 and 4 × 4 configurations are more suitable for field applications that require a high gain.

## IV. BEAMFORMING EVALUATION

In this section, the simulated and measured beamforming performances of the proposed array are presented, the method to construct the 360° smart beamforming antenna structure is illustrated, and the advantages over the relevant state-of-the-art antennas are identified.

### A. Simulation Results of the Proposed Beamforming Arrays

The beam steering capability of the proposed antenna arrays are simulated in CST by asserting the different phase shift for the signal traveling into P1 to P4. The phase shift for each parts P1/P2/P3/P4 are as follow, 0°/0°/0°/0° for 0° beam, 45°/180°/−45°/90° for −40° beam and 90°/−45°/180°/45° for +40° beam. The beam steering capability of the antenna arrays is shown in Fig. 20.

All the arrays (1 × 4, 2 × 4 and 4 × 4) demonstrate very similar steering capability of around ±41° at peak gain, and it shall cover ±45° steering beam when operating at 3 dB beamwidth.

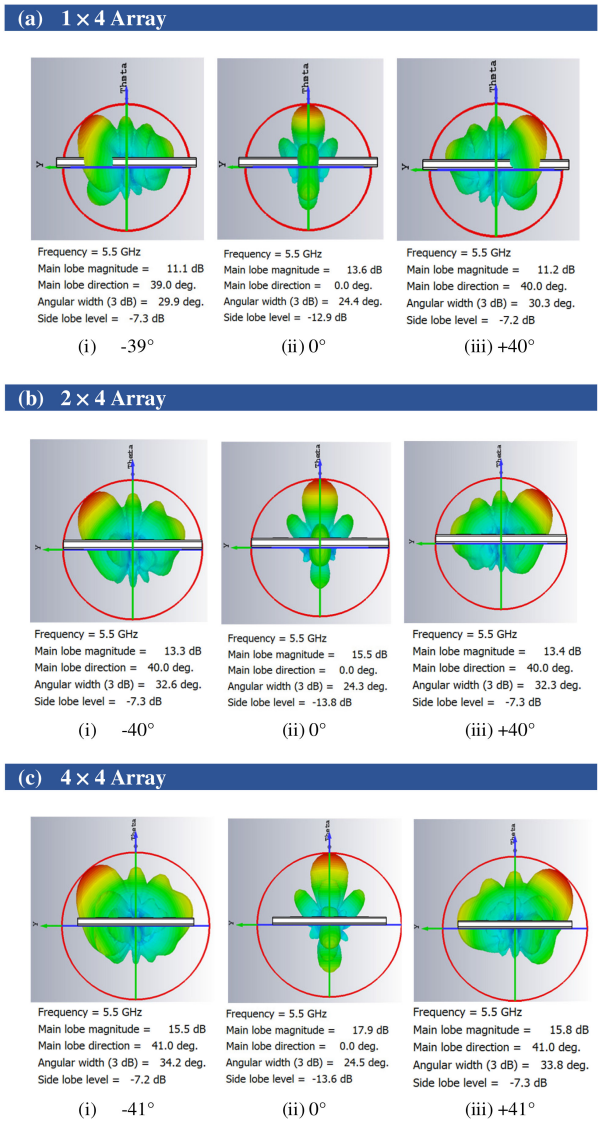


Fig. 20. CST simulated results of beam steering capability of the proposed antenna arrays.

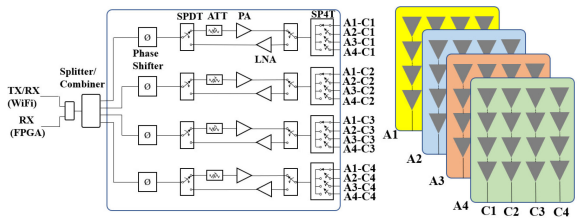


Fig. 21. Block diagram of the 4 × 4 beamforming antanna system.

### B. Experimantal Results of the Proposed Beamforming Arrays

The beamforming performance is evaluated using the beamforming structure as described in Fig. 21. The flexible structure consists of up to 4 units of 90° phase arrays (A1–A4) to cover the entire 360° service angle, each array consists of 4 horizontal feeding ports (C1–C4) to support beam steering in the 90° sector. The 4 units of 4 × 4 arrays with 16 antenna ports are supported

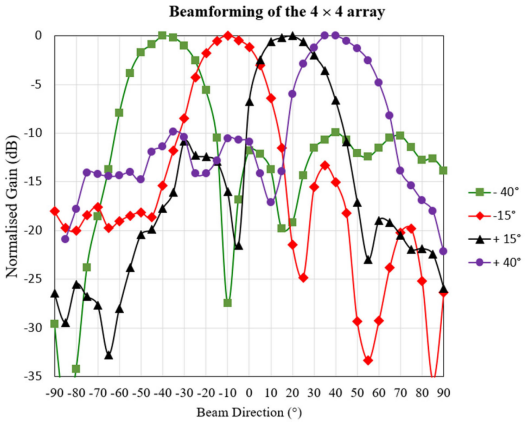


Fig. 22. Measurement results of the 4 × 4 beamfroming array.

TABLE IV
COMPARISON BETWEEN THE SIMULATED AND MEASURED RESULTS OF THE 4 × 4 BEAMFORMING ARRAY

| Beam Angle | | | - 40° | - 15° | 15° | - 40° |
|---|---|---|---|---|---|---|
| Antenna Gain | dBi | Simulated | 15.8 | 17.6 | 17.5 | 15.5 |
| | | Measured | 14.38 | 16.03 | 16.43 | 14.79 |
| Sidelobe Level | dB | Simulated | -7.3 | -12.0 | -11.6 | -7.2 |
| | | Measured | -9.95 | -13.34 | -12.25 | -9.84 |
| 3dB Beamwidth | ° | Simulated | 33.8 | 25.9 | 25.9 | 34.2 |
| | | Measured | 30.9 | 27.5 | 28.2 | 31.5 |

by 4 RF beamforming chains. The RF beamforming chains consist of a Single Pole Four Throw (SP4T) switch for antenna switching, each RF beamforming chain has two Single Pole Double Throw (SPDT) switches to toggle between the transmit and receive path, a 6-bit phase shifter with 5.625° resolution functions to vary the phase of each RF chain for antenna beam shaping, a Low Noise Amplifier (LNA) for receiver and a Power Amplifier (PA) for transmitter which were added to boost the RF signal and compensate the insertion loss exhibited by the phase shifter, SPDT, SP4T, and power combiner. The RF Attenuator (ATT) was populated to provide 30 dB dynamic transmit power range. The 4 RF chains are combined into a single RF port by a power combiner to interface with the radio transceiver, the antennas and transmitter/receiver switching can be controlled by Field Programmable Gate Array (FPGA) via Input-Output (IO) ports, Analog to Digital Converter (ADC) and Digital to Analog Converter (DAC) that directly interact with the circuit components inside the RF chains.

The beamforming is evaluated on one of the 4 arrays that services a 90° sector. The measurement environment and setup are described in Fig. 16 and Fig. 17. The beam steering result is presented in Fig. 22.

The measurement results are compared with the simulated result in Table IV. The measured result shows a fair agreement with the simulated results. Due to the identical arrays, similar result is expected for the rest of the 270° sector. With the 6-bit phase shifter resolution of 5.625°, the minimum resolution of the beam steering angle of the 4 × 4 array was simulated and measured with approximately 2°.

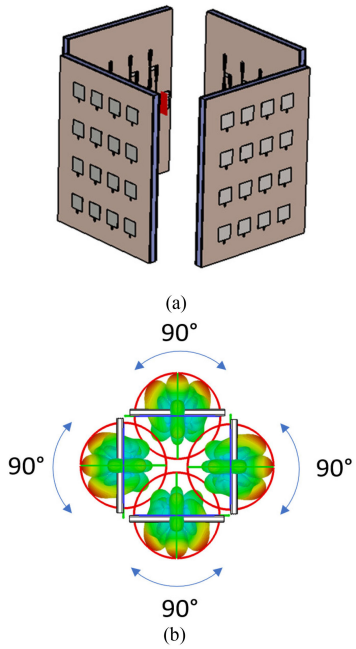


Fig. 23. The 360° beamforming antanna structure. (a) Isometric view. (b) Beamforming pattern of the 360° antenna structure

Up to 4 units of arrays can be integrated into a beamforming antenna system depending on the installation scenario requirements highlighted earlier in Fig. 1. The 360° beamforming structure is presented in Fig. 23, where Fig. 23(a) shows the isometric view of the flexible antenna structure and Fig. 23(b) illustrates the CST microwave studio simulation result of the beamforming pattern with the 4 units of 4 × 4 antenna arrays placed in a perpendicular manner, each of the array is dedicated to support 90° sector. Each sector can be configured to support i) 90° by activating 1 of the 4 antenna ports, or ii) beamforming with 25° beamwidth covering the 90° sector by activating all antenna ports with a different phase shift. The measured gain for each array was 14.38–17.25 dBi with the beamwidth of 20°–31.5° over the ±40° beam steering angle.

### C. Comparison With the State-of-the-Art Antennas

Table V highlights the comparison with the state-of-the-art wideband beamforming antenna systems that have the 360° steering capability in 802.11ac applications which could be the potential candidates for deployment in the scenarios presented in Fig. 1. As can be seen from the comparison, the antenna structure proposed in this work shows the following advantages over the literature, i) with the dual substrate structure, F4BTM-2 with $\varepsilon_r = 3$, $h = 1.56$ mm and air with $\varepsilon_r = 1$, $h = 6$ mm, the operating frequency bandwidth is effectively improved, which covers both the conventional 5 GHz ISM band 5.17 to 5.85 GHz as well as the 4.9 GHz licensed band, ii) the novel array structure that effectively combines the signal from each element results in a higher gain of 14.38 to 17.25 dBi compared to 10 and 12 dBi, which makes it more suitable for practical applications, iii) with flexible beam steering capability, each RF chain is controlled by a 6-bit phase shifter with 5.625° resolution,

TABLE V
COMPARISON WITH THE STATE-OF-THE-ART BEAMFROMING ANTENNA

| | [3] | [5] | This work |
|---|---|---|---|
| Type of Array Element | Electro-magnetic Bandgap | Circular Patch with Six Parasitic Elements | Dual Substrate Capacitive Feed MPA |
| Number of Arrays | 12 | 6 | 4 |
| Operating Frequency (GHz) | 5.18 – 5.825 | 5.1 – 5.9 | 4.9 – 5.9 |
| Antenna Array Gain (dBi) | 12 | 10 | 14.38 – 17.25 |
| Azimuth Beamwidth | 30° | 42° | 27.5° – 31.5° |
| Beam Steering Method | PIN Diode | PIN diode | SP4T and Phase Shifter |
| Beam Steering Resolution | 30° | 60° | Minimum 2° |
| Side Lobe Level (dB) (from antenna radiation graph) | - 6 – -12 | -7 | -9.8 – -13.3 |

iv) it has the advantage to pre-configure the antenna gain prior to the deployment, where the 1 × 4, 2 × 4 or 4 × 4 arrays can be pre-configured into the 360° beamforming antenna, and v) since each array covers a sector up to 90°, thus the proposed structure requires only 4 arrays for 360° coverage, with fine steering angle resolution that improves the accuracy of the beam focusing between the base station and the targeted clients.

## V. CONCLUSIONS AND FUTURE WORK

A novel antenna structure was proposed to cater for application needs in the dynamic automotive environment. The capacitive feed rectangular patch antenna with dual substrate was adopted for wideband operation, and the proposed element is able to deliver operating frequency from 4.9 to 5.9 GHz. The beamforming antenna array was created by integrating multiple single elements into a bigger array with 4 feeding ports for beam steering applications. In this work, 3 types of antenna array were designed to cater for different mobile application needs, and the proposed 1 × 4, 2 × 4 and 4 × 4 antenna arrays were simulated using CST software which were capable of performing ±40° beam steering. The antennas were fabricated using the standard PCB manufacturing process and then experimentally evaluated. The realized gain of the antenna is 11.16 dBi, 14.59 dBi, and 17.25 dBi respectively for the 1 × 4, 2 × 4 and 4 × 4 array. The array was integrated into a smart antenna system that provides 360° scanning capability. The measurement results for beam steering capability of the antenna array agreed well with the simulated results. The proposed smart antenna system is a good candidate for infrastructure deployment in the modern transportation market. The future work involves field trial on the proposed beamforming antenna structure in the real environment such as train to trackside and vehicle to roadside communication, and the front-end prototype which will then be miniaturized and productized for use in the future transportation market.

## ACKNOWLEDGMENT

The authors would like to acknowledge and express sincere appreciation to the Singapore Economic Development Board (EDB) and RFNet Technologies Pte. Ltd. for financing and providing a good environment and facilities to support the project.

## REFERENCES

[1] M. C. Tan, M. Li, Q. H. Abbasi, and M. Imran, "A smart and low-cost enhanced antenna system for industrial wireless broadband communication," in *Proc. 12th Eur. Conf. Antenna Propag. (EUCAP)*, London, U.K., 2018, pp. 1–4.

[2] C. Gu *et al.*, "Compact smart antenna with electronic beam-switching and reconfigurable polarizations," *IEEE Trans. Antennas Propag.*, vol. 63, no. 12, pp. 5325–5333, Oct. 2015, doi: 10.1109/TAP.2015.2490239.

[3] H. Boutayeb, P. R. Watson, W. Lu, and T. Wu, "Beam switching dual polarized antenna array with reconfigurable radial waveguide power dividers," *IEEE Trans. Antennas Propag.*, vol. 65, no. 4, pp. 1807–1814, Nov. 2016, doi: 10.1109/TAP.2016.2629469.

[4] Y. Y. Lin, C. L. Liao, T. H. Hsieh, and W. J. Liao, "A novel beam switching array antenna using series-fed slots with PIN diodes," *IEEE Antennas Wireless Propag. Lett.*, vol. 16, pp. 1393–1396, Dec. 2016, doi: 10.1109/LAWP.2016.2639046.

[5] Y. Yang and X. Zhu, "A wideband reconfigurable antenna with 360° beam-steering for 802.11ac WLAN applications," *IEEE Trans. Antennas Propag.*, vol. 66, no. 2, pp. 600–608, Dec. 2017, doi: 10.1109/TAP.2017.2784438.

[6] S. Krishna, G. Mishra, and S. Shama, "A series fed planar microstrip patch array antenna with 1D beam steering for 5G spectrum massive MIMO applications," in *Proc. IEEE Radio Wireless Symp.*, Anaheim, CA, USA, 2018, pp. 209–212.

[7] C. A. Balanis, "Microstrip and mobile communications antennas," in *Antenna Theory Analysis and Design*, 4th ed., Hoboken, New Jersey, USA: John Wiley & Sons, Inc., 2016, ch.14, sec. 14.2, pp. 788–823.

[8] G. Giunta, C. Novi, S. Maddio, G. Pelosi, M. Righini, and S. Selleri, "Efficient tolerance analysis on a low cost, compact size, wideband multilayer patch antenna," in *Proc. IEEE Int. Symp. Antennas Propag. USNC/URSI Nat. Radio Sci. Meeting*, San Diego, CA, USA, 2017, pp. 2113–2114.

[9] R. Gupta and M. Kumar, "Bandwidth enhancement of microstrip patch antennas by implementing circular unit cells in circular pattern," in *Proc. 5th Int. Conf. Comput. Intell. Commun. Networks*, Mathura, India, 2013, pp. 10–13.

[10] K. Mandal, L. Murmu, and P. P. Sarkar, "Investigation on compactness, bandwidth and gain of circular microstrip patch antenna," *IEEE Devices Integr. Circuit (DevIC)*, Kalyani, India, 2017, pp. 742–746.

[11] S. N. Ather, R. K. Verma, and P. K. Singhal, "Bandwidth enhancement for truncated rectangular microstrip antenna using stacked patches and defected ground structure," in *Proc. 5th Int. Conf. Comput. Intell. Commun. Networks*, Mathura, India, 2013, pp. 55–56.

[12] R. R. Selvaraju, M. R. Kamarudin, M. H. Jamaluddin, M. H. Dahri, and C. Y. Low, "Compact 4-element beam steerable printed adaptive array antenna for 5G application," in *Proc. Asia-Pacific Conf. Appl. Electromagnetics (APACE)*, Langkawi, Malaysia, 2016, pp. 30–33.

[13] Y. Wang, H. Wang, and G Yang, "Design of dipole beam-steering antenna array for 5G handset applications," in *Proc. Progress Electromagn. Res. Symp. (PIERS)*, Shanghai, China, 2016, pp. 2450–2453.

[14] M. Mantash and T. A. Denidni, "Millimeter-wave beam-steering antenna array for 5G applications," in *Proc. IEEE 28th Annu. Int. Symp. Personal, Indoor, Mobile Radio Commun. (PIMRC)*, Montreal, QC, Canada, 2017, pp. 1–3.

[15] J. H. Kim, J. H. Han, J. S. Park, and J. G. Kim, "Design of phased array antenna for 5G mm-wave beamforming system," in *Proc. IEEE 5th Asia-Pacific Conf. Antennas Propag. (APCAP)*, Kaohsiung, Taiwan, 2016, pp. 201–202.

[16] Y. Wang, L. Zhu, H. Wang, Y. Luo, and G. Yang, "A compact, scanning tightly coupled dipole array with parasitic strips for next-generationwireless applications," *IEEE Antennas Wireless Propag. Lett.*, vol. 17, no. 4, pp. 534–537, Apr. 2018, doi: 10.1109/LAWP.2018.2798660.

[17] S. A. Aghdam, J. Bagby, and R. J. Pla, "Design and development of linear array of rectangular aperture coupled microstrip antennas with application in beamforming," in *Proc. 17th Int. Symp. Antenna Technol. Appl. Electromagnetics (ANTEM)*, Montreal, QC, Canada, 2016, pp. 1–3.

[18] V. G. Kasabegoudar, D. S. Upadhyay, and K. J. Vinoy, "Design studies of ultra-wideband microstrip antennas with a small capacitive feed," *Int. J. Antennas Propag.*, vol. 2007, pp. 1–8, Dec. 2007, doi: 10.1155/2007/67503.

[19] J. Nasir, M. H. Jamaluddin, M. R. Kamarudin, I. ullah, Y. C. Lo, and R. Selvaraju, "A four-element linear dielectric resonator antenna array for beamforming applications with compensation of mutual coupling," *IEEE Access*, vol. 4, pp. 6427–6437, Oct. 2016, doi: 10.1109/ACCESS.2016.2614334.

[20] D. Pavithral, P. Ramya, K. R. Dharani, and M. R. Devi, "Design of microstrip patch array antenna using beamforming technique for ISM band," in *Proc. Fifth Int. Conf. Adv. Comput. (ICoAC)*, Chennai, India, 2013, pp. 504–507.

[21] M. S. R. Bashri, T. Arslan, and W. Zhou, "A dual-band linear phased array antenna for WiFi and LTE mobile applications," in *Proc. Loughborough Antennas Propag. Conf. (LAPC)*, Loughborough, U.K., 2015, pp. 1–5.

[22] C. Y. Cheng, H. Y. Huxie, and F. H. L. Su, "A compact high gain patch antenna array for IEEE 802.11ac MIMO application," in *Proc. IEEE 5th Asia-Pacific Conf. Antennas Propag.*, Kaohsiung, Taiwan, 2016, pp. 327–328.

[23] M. U. Khan and M. S. Sharawi, "A compact 8-element MIMO antenna system for 802.11ac WLAN applications," in *Proc. Int. Workshop Antenna Technol. (iWAT2013)*, Karlsruhe, Germany, 2013, pp. 91–94.

[24] S. A. Nasir, M. Mustaqim, and B. A. Khawaja, "Antenna array for 5th generation 802.11ac Wi-Fi applications," in *Proc. 11th Annu. High Capacity Opt. Networks merging/Enabling Technologies (Photon. Energy)*, Charlotte, NC, USA, 2014, pp. 20–24.

[25] W. S. Chen, C. Y. Hsu, and F. S. Chang, "Broadband three-element MIMO antennas for IEEE802.11ac," in *Proc. IEEE 5th Asia-Pacific Conf. Antennas Propag. (APCAP)*, Kaohsiung, Taiwan, 2016, pp. 267–268.

[26] C. A. Balanis, "Arrays and feed networks," in *Antenna Theory Analysis and Design*, 4th ed., Hoboken, New Jersey, USA: John Wiley & Sons, Inc., 2016, ch.14, sec. 14.8, pp. 832–837.

[27] S. D. Assimonis, T. Samaras, and V. Fusco, "Analysis of the microstrip-grid array antenna and proposal of a new high-gain, lowcomplexity and planar long-range WiFi antenna," *IET Microwaves, Antennas Propag.*, vol. 12, no. 3, pp. 332–338, Mar. 2018, doi: 10.1049/iet-map.2017.0548.

[28] A. Ghasemi, A. Abedi, and F. Ghasemi, "Introduction to radiowaves propagation," in *Propagation Engineering in Radio Links Design*, New York, USA: Springer, 2013, ch.1, sec. 1.10.1, pp. 26–27.

[29] 3ds.com. (2019), CST Studio Suite 3D EM simulation and analysis software. [Online]. Available at: https://www.3ds.com/products-services/simulia/products/cst-studio-suite/, Accessed on: Oct. 23, 2019.

**Moh Chuan Tan** received the B.Tech. degree in electronic engineering from the National University of Singapore, Singapore, in 2001. He is currently working toward the Ph.D. degree in electronic engineering with the University of Glasgow, Glasgow, U.K. From 1991 to 2001, he was with Kenwood Electronic Technologies Pte. Ltd., Singapore. He was a Land Mobile Radio Transceiver Designer, where he helped to set up the Kenwood R&D center in Singapore, developed and managed five models of land mobile radio product design including the Kenwood award winning model UBZ-LF14 in 1999 (a Family Radio Service radio transceiver for USA). In 2001, he joined RFNet Technologies Pte. Ltd., Singapore as a Pioneer Member where he had set up the R&D department and successfully designed many wireless LAN products for industrial applications such as automotive, railway, industrial IoT, etc. He is currently the Technical Director of R&D department who oversees the product and technology development. His research interests include smart antennasand RF modular frontends and systems.

**Minghui Li** (M' 08) received the B.Eng. and M.Eng. degrees from Xidian University, Xi'an, China, in 1994 and 1999, respectively, and the Ph.D. degree from Nanyang Technological University (NTU), Singapore, in 2004, all in electrical engineering. From 1994 to 1996, he was a Faculty Member with the School of Electronic Engineering , Xidian University. From 1999 to 2000, he was a Research Engineer with Siemens Ltd., China. From 2003 to 2008, he was first with the School of Electrical and Electronic Engineering and then with the Intelligent Systems Center, NTU as a Research Fellow. From 2008 to 2013, he was a Lecturer with the Department of Electronic and Electrical Engineering , University of Strathclyde, U.K. He joined the School of Engineering, University of Glasgow, U.K., as an Associate Professor in August 2013. His research interests include phased array systems, array design and processing, direction-of-arrival estimation, adaptive and arbitrary beamforming, spatial-temporal processing and coding, smart antennas, MIMO, evolutionary computation, wireless sensor networks, and coded ultrasound, with application to modern radar, underwater sonar, medical diagnosis, non-destructive evaluation, and wireless communications.

**Qammer H. Abbasi** (SM'16) received the B.Sc. and M.Sc. degrees in electronics and telecommunication engineering from the University of Engineering and Technology, Lahore, Pakistan, and the Ph.D. degree in electronic and electrical engineering from the Queen Mary University of London (QMUL), London, U.K., in 2012. In 2012, he was a Postdoctoral Research Assistant with the Antenna and Electromagnetics Group, QMUL. He is currently a Lecturer (Assistant Professor) with the School of Engineering, University of Glasgow, Glasgow, U.K. He has contributed more than 250 leading international technical journal and peer-reviewed conference papers, and eight books. He received several recognitions for his research, which include appearance on BBC, STV, dawnnews, local and international newspapers, cover of MDPI journal, most downloaded articles, U.K. exceptional talent endorsement by Royal Academy of Engineering, National Talent Pool Award by Pakistan, International Young scientist Award by NSFC China, URSI Young Scientist Award, National Interest Waiver by USA, four best paper awards, and best representative image of an outcome by QNRF. He is an Associate Editor for the IEEE JOURNAL OF ELECTROMAGNETICS, RF AND MICROWAVES IN MEDICINE AND BIOLOGY, IEEE SENSORS JOURNAL, IEEE OPEN ACCESS ANTENNA AND PROPAGATION, IEEE ACCESS and acted as a Guest Editor for numerous special issues in top notch journals.

**Muhammad Ali Imran** (M'03–SM'12) received the M.Sc. (Hons.) and Ph.D. degrees from Imperial College London, London U.K., in 2002 and 2007, respectively. He is the Dean of Glasgow College, UESTC and a Professor of communication systems with the School of Engineering, University of Glasgow, Glasgow, U.K. He is an Affiliate Professor with the University of Oklahoma, USA, and a Visiting Professor with the 5G Innovation Centre, University of Surrey, U.K. He has more than 18 years of combined academic and industry experience, working primarily in the research areas of cellular communication systems. He has been awarded 15 patents, has authored or coauthored more than 400 journal and conference publications, and has been principal or coprincipal investigator on more than £6 million in sponsored research grants and contracts. He has supervised more than 40 successful Ph.D. graduates. He has an award of excellence in recognition of his academic achievements, conferred by the President of Pakistan. He was also awarded the IEEE Comsoc's Fred Ellersick Award 2014, the FEPS Learning and Teaching Award 2014, and the Sentinel of Science Award 2016. He was twice nominated for the Tony Jean's Inspirational Teaching Award. He is a shortlisted finalist for The Wharton-QS Stars Awards 2014, the QS Stars Reimagine Education Award 2016 for innovative teaching, and VC's Learning and Teaching Award from the University of Surrey. He is a Senior Fellow of the Higher Education Academy, U.K. He is the Editor or Co-Editor of eight books.